Brodogradnja Volume 77 Number 3 (2026) 77307

University of Zagreb
Faculty of Mechanical
Engineering and Naval
Architecture

journal homepage: www.brodogradnja.fsb.hr

Brodogradnja

An International Journal of Naval Architecture and
Ocean Engineering for Research and Development

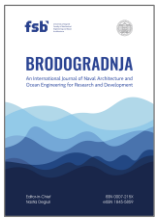

CFD approach to full-scale resistance: The Lucy Ashton case

Matija Vasilev[1,2*], *Milan Kalajdžić*[1,2], *Dmitriy Ponkratov*[3]

[1]*Department of Naval Architecture, Faculty of Mechanical Engineering, University of Belgrade, 11120 Belgrade, Serbia*
[2]*Ocean Pro Marine Engineers LTD, Belgrade, 11120 Belgrade, Serbia*
[3]*Siemens Digital Industries Software, London, UK*

ARTICLE INFO

Keywords:
Full-scale
Model scale
Resistance prediction

ABSTRACT

Accurate prediction of ship resistance remains a major challenge in Computational Fluid Dynamics (CFD), particularly when translating results from model to full scale. This study investigates the prediction of total resistance for the historic vessel Lucy Ashton using CFD across six model scales and full scale. Experimental resistance data were harmonized using third-order polynomial fits, enabling consistent comparison with CFD results. Two full-scale approaches were evaluated: Setup 1 with prescribed inflow and Setup 2 incorporating surge motion with applied thrust to emulate deck-mounted jets used during sea trials. Across all scales, CFD predictions showed strong agreement with experiments, with deviations typically within ±5%, consistent with accepted validation standards. Dynamic motions (heave and pitch) were also examined, and both setups produced nearly identical trends, with absolute differences negligible for resistance assessment. The results demonstrate that both CFD methodologies provide reliable full-scale resistance estimates.

1. Introduction

The improvement of ship performance (energy efficiency) as a global agenda goal was first presented in 2018 through [1]. The adoption of [2] finally defined the goal set by the International Maritime Organization (IMO), which is to reduce global greenhouse gas (GHG) emissions to net-zero by 2050. Checkpoints have also been introduced for 2030 and 2040, by which time total annual GHG emissions from international shipping should be reduced by at least 20%, striving for 30%, by 2030 and by at least 70%, striving for 80%, by 2040 compared to 2008 levels. Moreover, peak emissions should be reached as soon as possible and the reduction of annual GHG emissions must achieve net-zero by 2050, compared to 2008. According to available data from [3] and [4], the reduction rate of CO_2 emissions from ships in global emissions for the period from 2008 to 2018 was 0.3%. The current phase involves the analysis of the post-2018 period, with the latest CO_2 emission data expected to be published in the Fifth IMO Greenhouse Gas Study 2025. Using another available source for now [5], the share of international shipping in global emissions was 7.5% in 2023, which is significantly higher than in 2018 when it was 2.89%.

* Corresponding author.
E-mail address: matija@oceanpro.eu

https://doi.org/10.21278/brod77307

Received 23 September 2025; Received in revised form 15 December 2025; Accepted 21 December 2025
Available online 28 December 2025
ISSN 0007-215X; eISSN 1845-5859

Due to the rapid increase in the share of global emissions, modern software tools are increasingly used in the shipbuilding industry, such as CFD [6], Artificial Neural Network (ANN) [7, 8] and since 2018, Artificial Intelligence (AI) [9] to accelerate ship optimization solutions. In addition to these approaches, various optimization algorithms have also been developed and successfully applied to ship design problems in order to further improve hydrodynamic performance and energy efficiency [10]. One of the biggest challenges in using CFD software is the reliability of the results, i.e., how trustworthy the computer-generated solutions are. In shipbuilding practice, model tests have been conducted for decades and their results have never been questioned. The results obtained from model tests are then extrapolated to full-scale dimensions following the guidelines provided in [11]. CFD software have been under development for over five decades and supporting guidelines are issued by the International Towing Tank Conference (ITTC) under reference document number 7.5-03, which covers resistance, propulsion and maneuverability. It was only in 2022 that the IMO included numerical calculations as an acceptable method for determining the reference speed for the Energy Efficiency for Existing Ship Index (EEXI) regulation framework [12, 13] with direct guidelines published in [14].

Of the 14 papers considered as benchmarks for CFD validation [15], only one vessel has full-scale data available - the general cargo ship Regal. This vessel was also the subject of the first CFD workshop related to a full-scale ship, organized by Lloyd's Register in 2016 [16]. The same author previously worked on a similar topic, validating CFD results against full-scale sea trial measurements [17, 18]. CFD workshops are characterized by the fact that measurement data (whether from model tests or full-scale) are not shared publicly until participants submit their results to the organizer. The workshop organizer holds the right to analyze all submitted data and compare it with experimental results. This method of organizing workshops is considered the only valid and correct approach. Over the past decades, several such workshops have been held, starting in 1980, followed by events in 1990, 1994, 2000, 2005, 2010, 2015, 2024 and another is known to be planned for 2025. The analysis of published results from the Lloyd's Register workshop showed that the mean comparison error of the predicted power was 13% for all submitted results, with only three out of 27 participants achieving errors below 3% for all considered speeds [16]. A deviation of up to 16% in total resistance between participants was also reported in another results analysis of the Lloyd's Register workshop [19].

Among the guidelines issued by the ITTC, one document specifically addresses uncertainty analysis in CFD verification and validation [20] in this document, numerical error is divided into four components: (iteration number, grid size, time step and other parameters). Among these, the grid size error is identified as the most significant contributor. Grid uncertainty stems from multiple factors related to grid generation, such as cell type and refinement strategy. These factors significantly influence the accuracy of flow field representation in maritime environments, making proper grid resolution a critical aspect in CFD analysis for ship hydrodynamics.

In the paper [21], the authors investigated the influence of grid size (ranging from 5 to 11 million cells) on the predicted self-propulsion propeller revolutions rate for two ships. The study resulted in a 0.15% uncertainty for the general cargo ship Regal and 4.02% uncertainty for the car carrier. However, the authors did not follow the guidelines for uncertainty analysis as specified by ITTC in [20] where it is recommended that the grid refinement ratio should be uniform and equal to $\sqrt{2}$. In the study by [22] the grid refinement ratio value of $\sqrt{2}$ was used for grid sensitivity analysis, covering four grids (12.3, 25.4, 41.1 and 62.5 million cells). This study again examined the Regal ship, but it remains unclear why the authors conducted analyses of the grid size effect on the total resistance coefficient, as the total resistance for this ship was not directly measured but was an average value from workshop participants. The authors reported deviations of the total resistance coefficient from the average value ranging from -6.27% to +0.44% between the coarsest and finest grids. The group of authors [23] in their study also performed a grid uncertainty analysis for the KVLCC2 ship using three grids (0.897, 1.69 and 3.077 million cells). They obtained an uncertainty of 2.49%, with results varying between -1% and +2% compared to experimental data. An extensive verification and validation study of ship scale CFD self-propulsion simulations is presented in [24]. As a part of the study, a speed and power test were conducted with a research vessel for three different power settings. Numerical uncertainties

due to the finite number of cells were assessed according to the grid convergence index (GCI) method. The observed uncertainty values were low, ranging from 0.54% to 4.52% (for grid ranges from 1.75 to 11.52 million of cells). The propeller revolution results aligned well with the trial data, with relative errors between -2.46% and -4.40% when compared to the corrected trial values. However, significantly larger errors were noted in the delivered power comparison, varying from -30.15% to -41.93%. In [25] RANS-CFD analyses employed to predict resistance, open water propeller performance and self-propulsion for a tanker ship, with results compared to experimental data and sea-trial measurements of three sister ships. The proposed methodology showed good agreement with full-scale power predictions, achieving a maximum error of 4.13%. Numerical uncertainty on resistance and thrust was approximately 0.5% for a grid of 9.9, 15.5 and 22.6 million cells, while the propeller torque uncertainty, identified as the major contributor, was calculated at 5%.

In the article written by [17] an optimized setup was determined based on Regal test case, balancing computational cost and accuracy, with an optimal mesh density of around 11 million cells. The findings emphasize the need for a separate full-scale ship CFD guideline, as using model scale parameters can lead to unnecessary computational resource waste. The study [26] combines numerical simulations and experimental tests to predict self-propulsion points and required brake power for a bulk carrier at full scale under different load conditions. The numerical results using the RKE turbulence model and a coarse mesh (4.1 million cells) showed good agreement with extrapolated towing tank data.

In [27] CFD simulations of delivered power are validated for a full-scale ship and verifies the numerical method through systematic grid refinement for both model and full-scale cases. With a validation uncertainty of 7% and an average comparison error of 1% in the speed range of 12.5 to 14.5 knots, the results highlight the accuracy of the simulations, particularly considering surface roughness effects on the hull and propeller.

In [28] the feasibility of full-scale CFD predictions for self-propulsion characteristics is demonstrated, applying a methodology to the KRISO container ship (KCS) that includes three full-scale simulations: open water, towed and self-propelled cases. It highlights key differences between model and full-scale simulations, particularly due to Reynolds number effects, with a thinner boundary layer in full scale leading to improved propeller performance and higher efficiency.

In [29] the nominal wake at full scale for a Handymax bulk carrier using CFD simulations with and without wall functions is assessed. A verification study showed small numerical uncertainties for frictional resistance and three turbulence models (RKE, SSTKO and RSM) were tested, with RSM providing the best agreement with experimental wake data. Significant scale effects were observed, with numerically obtained effects exceeding extrapolated ones, particularly when using wall functions at model scale.

The literature review highlights several studies that compare the performance of different types of ships, using both CFD analysis and experimental methods. These studies often involve model testing, as well as full-scale measurements of ship speed and power. Additionally, many of these works consider the influence of various factors, such as the number of cells and cell size in CFD simulations, on the accuracy of the results. The problem in estimating resistance in full scale lies in the method used to extrapolate results from model tests to real-world conditions. Today, two well-established methods known as ITTC 57 and ITTC 78, dating back over 50 years, are still commonly used for this purpose [11]). These methods, although originating in the past, continue to be relevant and widely applied in current practice. So, CFD results are not directly compared with measured data but rather with extrapolated values. It is true that these methods have been used in shipbuilding practice for decades and that designed ships have shown that extrapolators can be trusted. However, whether a specific numerical value, such as the engine power required at a given sailing speed, can be trusted is quite difficult to determine due to numerous parameters (such as the effect of the propeller's operation behind the ship and weather conditions) that can influence the ship's performance. Therefore, the best method of comparison is to conduct direct resistance measurements of the full-scale ship alongside CFD results.

One of the main challenges in full-scale resistance measurement is the difficulty in directly measuring resistance on a full-size ship. To address this, one common approach involves towing the ship (without a propeller) with one or two tugboats and measuring the force exerted on the towline. However, a major

limitation of this method is that the tugboats pulling the ship affect the resistance measurement. Their wake and wave patterns, generated as they move ahead of the towed ship, influence the resistance of the ship being towed. This interaction introduces a level of complexity that must be accounted for when interpreting the results, but it is not clear how.

An alternative method to measure ship resistance involves the installation of jet engines on the ship's deck. This approach creates thrust, simulating propulsion, while eliminating the influence of the tugboats' waves. Two historical cases of such experiments, which were conducted several decades ago, are documented in the literature and published in two separate papers [30, 31].

The primary goal of the measurements of the hull resistance of the Lucy Ashton [30] was to gather data for comparing ship resistance with the resistance predicted from model tests across a wide range of speeds. By obtaining accurate resistance values, the comparisons could be made between these values and the corresponding model test resistance, which would help clarify the effectiveness of various methods used for skin friction correction between the model and ship. Additionally, the tests aimed to explore how factors like fairing seams, different ship surfaces, paint deterioration and appendages such as twin-screw bossings or "A" brackets with shafts affect resistance. The research program was developed with these objectives in mind, with some adjustments based on experience gained during testing. The analysis and testing have been further expanded and published in three additional parts. The paper [32] focuses on correlating the measured full-scale resistance of the Lucy Ashton with the results from tests on six geometrically similar models, ranging from 9 to 30 feet in length. The translation of model test results to full scale was done using Froude's skin-friction coefficients and skin-friction formulations. The study specifically correlates resistance for four naked hull conditions, including tests with two different paint surfaces and the effect of fairing the seams of the shell plating. The paper also describes the various corrections applied to the ship results and provides an analysis of the hull surface roughness measurements. Next part [33] examines the resistance increments caused by twin-screw shaft appendages (bossings and shaft brackets) on the Lucy Ashton, correlating full-scale ship results with those from six geometrically similar models. The study focuses on measuring additional resistance due to these appendages, marking the first time this has been done on a full-size ship. The findings are analyzed in the context of scale effects on appendage resistance. This final part [34] presents additional investigations on the Lucy Ashton, covering the effects of fouling on resistance, acceleration and retardation trials to determine the ship's virtual mass and Pitot traverses in the frictional belt to study velocity distributions under various hull-surface conditions.

The Lucy Ashton case is investigated through the paper published by [35]. In this study numerical simulations were performed across various Froude numbers and scaling ratios, primarily assuming a smooth hull and fixed position. A major challenge identified was the smearing of the free surface near the hull, which led to underpredicted resistance values-especially at full scale-due to artificially low viscosity. Including effects like surface roughness and freedom in heave and pitch improved agreement with experimental data. The study also highlighted limitations of the double-body approach at higher Froude numbers and found inconsistencies in form factor estimation using Prohaska's method. The ITTC 78 scaling procedure matched full-scale results well when roughness and air resistance were excluded. The study [36] found that CFD generally predicted lower resistance than 1950s experimental data due to assumptions of a smooth hull and no heave or pitch. Scatter in full-scale resistance decreased with increasing Froude number, with a median absolute deviation up to 2.3%, and the variability was similar to that observed at model scale, supporting confidence in full-scale CFD predictions.

In 1967, the R.V. Meteor [31] conducted full-scale tests in the Baltic Sea to validate the extrapolation of model test results to full-scale conditions for large, fast vessels. The tests included a model family of the ship at scales of 1:25, 1:19 and 1:13.75, with the aim of completing the series with full-scale data. Key measurements focused on resistance, propeller thrust, propeller power demand and the wake both in the absence and presence of the propeller. Boundary layer velocity distribution and ship behavior during maneuvering were also studied. After completing the measurement of speed and power trials, the propeller was removed to measure the total resistance. The Meteor was equipped with three jets (inspired by Lucy Ashton case) with a total power of 12000 HP. Jet thrust was measured by a strain gauges installed in the

supporting frame of each jet. Other measurements included wake using pitot tubes, boundary layer data with Prandtl tubes, rudder forces with a balance on the rudder shaft and ship speed through calibrated current meters. The results indicated that the ITTC 1957 line, commonly used for frictional resistance extrapolation, had too small a slope. The total efficiency of the model and prototype were identical and the thrust deduction fraction showed no dependence on scale. The study confirmed laboratory values for the boundary layer law, with $K = 0.41$ and $C = 5.0$.

The subject of this study is the Lucy Ashton case because it was used for the blind CFD workshop organized in 2024 by Chalmers University of Technology, in which the authors participated. The Lucy Ashton, originally a Clyde paddle steamer built in 1888, was modified for ship resistance experiments after its retirement in 1949. The vessel underwent significant alterations, including the removal of paddle wheels, machinery and deckhouses, followed by the addition of sand ballast and structural reinforcements. The hull was cleaned, smoothed with fairing material and sharpened at the plate edges to improve hydrodynamic performance. To achieve the required thrust for resistance tests, four Rolls Royce Derwent V jet engines were installed on a specially constructed gantry. These engines provided a combined thrust exceeding six tons, enabling the ship to reach speeds of about 15 knots. Since the jet engines could not reverse thrust, large steel flaps were added beneath the gantry to act as emergency water brakes, effectively slowing the vessel. A soundproof cabin was constructed to protect the crew from the intense noise. Accurate thrust measurement systems were installed using strain gauges on the engine mounts to ensure precise resistance readings. The choice of jet engines provided a steady and controllable thrust, overcoming issues like wake interference and unstable towing forces seen in alternative methods. Additional fuel tanks were fitted to extend operational range and ensure uninterrupted test runs on the measured mile.

The workshop cases were chosen based on data from 1950s sea trials, which included tests at various speeds and with four different surface conditions. These conditions involved two types of coatings: aluminum paint and red oxide paint, along with sharp and faired seams. For the workshop, participants were instructed not to include roughness modeling in their CFD simulations. Consequently, the smoothest experimental condition - faired seams with aluminum paint - was used as the reference for comparison. This condition was also used to determine the specific speeds selected for the simulations.

Two pitot logs were installed on the hull: one 72 ft 6 in. and the other 97 ft 4 in. aft of the forward perpendicular. These logs measured both static and dynamic pressure heads, connected to a mercury manometer to determine water speed. The logs could extend up to 3 ft from the hull's surface for boundary layer velocity measurements. Although their primary purpose was boundary layer investigation, these logs were also used to measure speed during acceleration and retardation trials. The calibration process involved taking readings during double runs on the measured mile, adjusting the log's position along the way. While fully extended readings were stable, issues arose with unstable data during traversing. Results were only considered reliable if the data scatter was within ±3% and enough readings were available for a mean curve. The data showed a thicker boundary layer (18 in.) at the No. 2 log's position compared to the No. 1 log's position (12 in.), reflecting the expected increase in boundary layer thickness along the hull at a speed of 10.18kn (unfortunately, data are available only for this speed) at the center line. Frictional-resistance coefficient derived from this velocity profile aligned well with direct resistance measurements.

Based on the results of conducted Lucy Ashton case, the objectives of this study are defined as follows:

- To compare CFD predictions with full-scale experimental measurements and scale-model tests performed with two degrees of freedom (heave and pitch) using the classical simulation approach in which the inflow passes around a fixed-speed ship.
- To compare CFD predictions with full-scale experimental measurements conducted with three degrees of freedom (surge, heave, and pitch) while explicitly accounting for the thrust generated by the jet engines.

2. Methodology

2.1 Case description

The Lucy Ashton case is highly suitable for developing the points mentioned earlier for several reasons:

- Data on total resistance from model tests is available for six different scales and multiple speeds: λ = [21.167, 15.875, 11.906, 9.525, 7.938 and 6.35];
- Data on total resistance for multiple speeds in full scale (λ = 1);

The basic data and dimensions of the Lucy Ashton ship are provided in the following Table 1, while the lines plan is provided in Fig. 1:

Table 1 Ship particulars

L_{pp} [m]	58.1
L_{wl} [m]	59.49
B [m]	6.4
T [m]	1.584
H [m]	2.1844
WS_{total} [m^2]	417
Δ [t] (sw)	390
C_b [-]	0.685
C_p [-]	0.705
C_m [-]	0.972

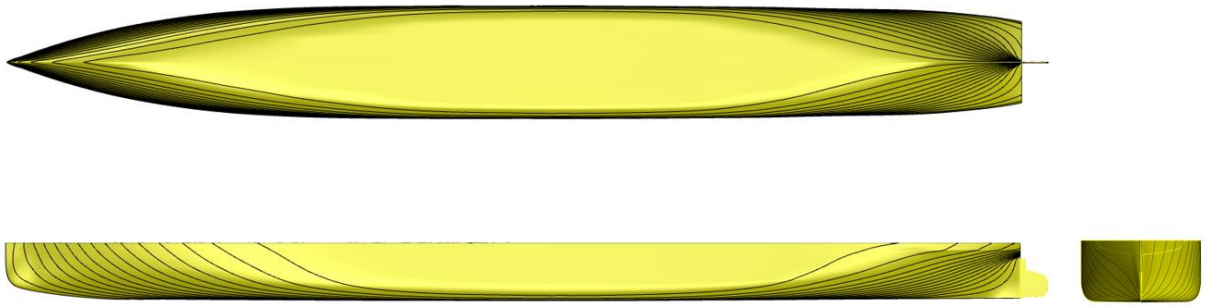

Fig. 1 Lines plan (Lucy Ashton)

2.2 CFD setup and simulation conditions

Setup 1: In the first (classical) CFD configuration, the ship has two degrees of freedom (heave and pitch), while the inflow velocity is imposed and water flows around the hull. The simulation is terminated when the total resistance, heave and pitch exhibit convergence. This setup is applied to all model scales and full-scale ship.

Setup 2: In the second CFD configuration, the ship has three degrees of freedom (surge, heave and pitch).The water domain is static, and a prescribed force, corresponding to the total thrust produced by the jet engines is applied at the location where the jets were mounted during the experiments. The entire computational domain translates with the vessel. The simulation stops once the ship speed, total resistance, heave and pitch converge. This setup is applied only for full-scale ship.

The cases considered in the workshop for the full-scale ship resistance prediction included following Fr = [0.130, 0.173, 0.219, 0.260, 0.304] and Fr = 0.219 for the model scales resistance prediction. In this

study, the number of conducted simulations were increased to contain all cases. Another distinction between this study and the simulations performed during the workshop is the inclusion of dynamic motions, specifically heave and pitch, which are now fully accounted for. For the CFD calculations, the software STAR-CCM+ developed by Siemens was used. In Table 2, "o" marked cells contain simulations conducted during the workshop, while with "x" are denoted additional simulations carried out in this study. Forces that are applied in Setup 2 are F=[2.25 kN, 4 kN, 7.5 kN, 12.5 kN, 23.5 kN] and it is important to note that values correspond to half-body. The location point where each force is applied is 19m from the aft perpendicular, in centerline and 3.216m above keel. The force location point moves together with a ship.

Table 2 Conducted simulations

λ	Fr=0.130	Fr=0.173	Fr=0.219	Fr=0.26	Fr=0.304
21.167	x	x	o, x	x	x
15.875	x	x	o, x	x	x
11.906	x	x	o, x	x	x
9.525	x	x	o, x	x	x
7.938	x	x	o, x	x	x
6.35	x	x	o, x	x	x
1	o, x	o, x	o, x	o, x	o, x

The kinematic viscosity can be determined based on the temperature of the water in which the experiments were conducted. In this case, it was determined based on known values for density and dynamic viscosity (given in Table 3).

Table 3 Water and air properties

	Full scale	Model scale
ρ_w [kg/m^3]	1026.02	998.8
ρ_a [kg/m^3]	1.225	1.242
η_w [Pas]	1.22E-03	1.27E-03
η_a [Pas]	1.79E-05	1.77E-05

2.3 Numerical models

The governing equations are discretized using the collocated Volume of Fluid (VOF) multiphase method integrated within the software. This method is designed for large-scale two-phase flows, specifically involving water and air, commonly encountered in naval hydrodynamics. The model describes a two-phase, incompressible, turbulent and viscous flow.

The VOF multiphase Eulerian model in STAR-CCM+ belongs to the interface-capturing methods category, which predicts the distribution and movement of the interface between immiscible phases. This approach assumes that the mesh resolution is adequate to capture the position and shape of the phase interface accurately. For more detailed insights into the VOF method, refer to [37]. A key characteristic of immiscible phase systems, such as air and water, is that the fluids remain separated by a distinct interface. To replicate the convective transport of immiscible fluid components, the High-Resolution Interface Capturing (HRIC) scheme is employed, ensuring precise tracking of sharp interfaces.

Fluid domain dimensions are defined as follows (from Aft Perpendicular):

- Inlet: 2.5 L_{pp} - defined as velocity inlet;
- Outlet: 3 L_{pp} - defined as pressure outlet with wave damping boundary option included;
- Bottom: 1.5 L_{pp} - defined as velocity inlet;
- Top: 1 L_{pp} - defined as velocity inlet;
- Port Side: 2 L_{pp} - defined as velocity inlet with wave damping boundary option included;

• Starboard Side: at centerline of the ship defined as symmetrical plane.

The wave damping length (*WDL*) is defined as two wave lengths (*WL*), where the wave length is calculated as per:

$$WL = 2\pi \cdot Fr^2 \cdot L_{pp} \tag{1}$$

The hull is considered as a no-slip wall as per [14] and a blended wall function is set as a default physics setting in the used software when *all y+ wall treatment* model is activated. In the user manual of used software is noted that *all y+ wall treatment* approach should be chosen whenever is available when complex geometries are being considered.

Principally, the flow is calculated only around the Port side of the ship to reduce computational resource consumption due to the large number of simulations and this condition was also defined through the workshop. The difference compared to the workshop guidelines is that dynamic pitch and heave are enabled, so the results obtained in this study are more reliable and differ from those sent by the authors to the organizers for participation in the workshop.

The turbulence model that is applied in this study is *k-ω* SST [38].

2.4 Grid uncertainty and post-processing

A grid convergence study is performed to assess the convergence of the results by systematically refining the base cell size by multiplying with $1/\sqrt{2}$ and 1/2. The convergence ratio is defined as:

$$R = \frac{\varepsilon_{21}}{\varepsilon_{32}} \tag{2}$$

where ε_{21} is the difference between the solution obtained using medium and fine mesh and ε_{32} is the difference between the solution obtained using coarse and medium mesh. *R* is used for the estimation of the convergence conditions: monotonic convergence is achieved when $0 < R < 1$, oscillatory convergence is achieved when $-1 < R < 0$ and divergence is achieved when $|R|>1$. The numerical uncertainty (U_G) and error (E) for monotonic convergence conditions is estimated as per ITTC [20]. The estimated order of accuracy (p_{RE}) and error (δ_{RE}) is calculated as per:

$$p_{RE} = \frac{\ln\left(\varepsilon_{32}/\varepsilon_{21}\right)}{\ln\sqrt{2}} \tag{3}$$

$$\delta_{RE} = \frac{\varepsilon_{21}}{\left(\sqrt{2}\right)^{p_{RE}} - 1} \tag{4}$$

To estimate the grid uncertainty U_G, a safety factor approach is employed [39], defining U_G as:

$$U_G = FS \cdot \left|\delta_{RE}\right| \tag{5}$$

where *FS* is a safety factor estimated as per [40]:

$$FS = 2.45 - 0.85P \text{ for } 0 < P \leq 1 \tag{6}$$

$$FS = 16.4P - 14.8 \text{ for } P > 1 \tag{7}$$

where *P* is the ratio of the estimated order of accuracy to the theoretical order of accuracy (p_{th}) which is two:

$$P = p_{RE}/p_{th} \tag{8}$$

Numerical uncertainty (U_{SN}) in this case is adopted to be equivalent to grid uncertainty:

$$U_{SN} = U_G \tag{9}$$

To determine if validation has been achieved, comparison error E is compared to validation uncertainty U_V given by:

$$U_V^2 = U_D^2 + U_{SN}^2 \tag{10}$$

where U_D is data uncertainty, but in Lucy Ashton case U_D is not available, therefore in this case validation uncertainty is equal to grid uncertainty. The comparison error is given by difference in the data D and simulation S values:

$$E = D - S \tag{11}$$

If $|E| < U_V$, the validation is achieved at the U_V level.

In the Lucy Ashton case grid uncertainty analysis had been done for two different scales in Lucy Ashton case (λ=21.167 and λ=1) and one speed.

In the numerical simulations conducted for Lucy Ashton full scale study, the direct consideration of the roughness effects is not included. However, this effect is accounted for in the post-processing stage by following the recommended procedures and guidelines outlined in [41]. The ITTC guidelines provide specific methodologies for incorporating the effects of the roughness and air resistance into the analysis, allowing for an assessment of the overall performance and characteristics of the ship. The roughness allowance (ΔC_F) is calculated as per [42]:

$$\Delta C_F = 0.044\left[\left(\frac{k_s}{L_{wl}}\right)^{\frac{1}{3}} - 10\mathrm{Re}^{-\frac{1}{3}}\right] + 0.000125 \tag{12}$$

where k_s is the surface roughness and it is known for Lucy Ashton (5.842×10^{-5}m) [34]. However, this value gives negative ΔC_F calculated as per Eq. 12, so the other approach is set because there is available the allowance on C_F, i.e., ΔC_F necessary to complete the full-scale ship-model balance, in the same document. Roughness allowances are given in Table 4 for each considered speed:

Table 4 Roughness allowances

Fr [-]	$\Delta C_F \times 10^3$ [-]
0.130	0.0181
0.173	0.0169
0.219	0.1303
0.260	0.2421
0.304	0.2979

The air resistance was neglected, as the superstructure had been removed prior to the sea trials. The additional structure installed to support the jet engines was lattice steel construction, resulting in minimal aerodynamic influence.

3. Results

The experimental datasets were fitted using third-order polynomial curves, achieving an R^2 value greater than 0.999 for each scale. This fitting procedure was necessary to enable a direct and consistent comparison between the CFD-based results and the experimental measurements. All experimental measurements of total resistance, both for the model and the full-scale ship, were converted into the non-dimensional total resistance coefficient using the available density values for fresh and seawater. The wetted surface area was estimated from the 3D hull model and consistently applied in the evaluation of the total resistance coefficient for both the experimental data and the CFD results. Furthermore, the standard deviation of the discrepancy between the polynomial-based values and the corresponding experimental measurements was determined for each scale, providing a quantitative measure of the fitting accuracy. The calculated standard deviations for all scales are presented in Table 5.

Table 5 Standard deviation of residuals between polynomial-fitted and experimental total resistance coefficients for each scale

λ [-]	σ [%]
21.167	2.20
15.875	2.30
11.906	2.90
9.525	2.30
7.938	1.20
6.350	2.00
1	3.10

3.1 Model scales

This section presents the CFD results obtained using Setup 1. In this context, the CFD results correspond to the total resistance coefficient evaluated for the half-hull at five Froude numbers. These coefficients are directly compared (relative error is given) with the experimental total resistance coefficients, which were obtained by applying the fitted polynomial to the measured total resistance data in each model scale.

In Tables 6-11 are given total resistance coefficients (C_T x 10^3) evaluated through Experimental Fluid Dynamics (EFD) and CFD for each *Fr* and relative error for model scales of 21.167, 15.875, 11.906, 9.525, 7.938 and 6.35, respectively.

Table 6 Results of Lucy Ashton case (model scale – λ=21.167)

Fr [-]	$C_{T,\mathrm{EFD}}\cdot 10^3$ [-]	$C_{T,\mathrm{CFD}}\cdot 10^3$ [-]	*E* %*D*
0.130	4.417	4.625	−4.7
0.173	4.278	4.451	−4.0
0.219	4.337	4.439	−2.3
0.260	4.615	4.675	−1.3
0.304	5.578	5.628	−0.9

Table 7 Results of Lucy Ashton case (model scale – λ=15.875)

Fr [-]	$C_{T,\mathrm{EFD}}\cdot 10^3$ [-]	$C_{T,\mathrm{CFD}}\cdot 10^3$ [-]	*E* %*D*
0.130	4.070	4.276	−5.1
0.173	3.963	4.102	−3.5
0.219	4.091	4.150	−1.4
0.260	4.388	4.484	−2.2
0.304	5.379	5.451	−1.3

Table 8 Results of Lucy Ashton case (model scale – λ=11.906)

Fr [-]	$C_{T,\mathrm{EFD}}\cdot 10^3$ [-]	$C_{T,\mathrm{CFD}}\cdot 10^3$ [-]	*E* %*D*
0.130	3.775	3.969	−4.6
0.173	3.741	3.758	−0.4
0.219	3.813	3.791	0.6
0.260	4.140	4.107	0.8
0.304	5.240	5.252	−0.2

Table 9 Results of Lucy Ashton case (model scale – λ=9.525)

Fr [-]	$C_{T,EFD}\cdot10^3$ [-]	$C_{T,CFD}\cdot10^3$ [-]	E %D
0.130	3.552	3.717	−4.6
0.173	3.533	3.534	0.0
0.219	3.648	3.629	0.5
0.260	3.947	3.878	1.7
0.304	5.041	5.051	−0.2

Table 10 Results of Lucy Ashton case (model scale – λ=7.938)

Fr [-]	$C_{T,EFD}\cdot10^3$ [-]	$C_{T,CFD}\cdot10^3$ [-]	E %D
0.130	3.393	3.524	−3.9
0.173	3.468	3.362	3.1
0.219	3.515	3.449	1.9
0.260	3.956	3.815	3.6
0.304	4.958	4.940	0.4

Table 11 Results of Lucy Ashton case (model scale – λ=6.350)

Fr [-]	$C_{T,EFD}\cdot10^3$ [-]	$C_{T,CFD}\cdot10^3$ [-]	E %D
0.130	3.257	3.399	−4.4
0.173	3.346	3.250	2.9
0.219	3.505	3.344	4.6
0.260	3.781	3.680	2.7
0.304	4.938	4.848	1.8

The grid uncertainty analysis was performed for the smallest model (λ=21.167) and the lowest speed (Fr=0.130), using three different cell sizes to generate the coarse, medium and fine meshes. The resulting total resistance coefficients obtained from these three mesh densities, along with the corresponding number of cells in the computational domain covering the half-hull, are presented in Table 12.

Table 12 Grid uncertainty analysis (λ=21.167, Fr=0.130)

	Coarse (S_3)	Medium (S_2)	Fine (S_1)
$C_{T,CFD}$ x 10^3 [-]	4.625	4.498	4.412
No. of cells x 10^6	0.63	1.311	2.637

Grid uncertainty in this case is 7.7% and since it is bigger than comparison error (4.7%), the validation is achieved.

3.2 Full-scale

Two different simulation setups were carried out to compare the CFD-based predictions of ship resistance, expressed through the total resistance coefficient. In both cases (Setup 1 and Setup 2), the computed total resistance coefficients were compared with the corresponding values obtained from the fitted polynomial representation of the experimental data (see Table 13 and Table 14). In addition to the resistance results, the dynamic motions (heave and pitch) were also evaluated, and the differences between the two setups are presented as well in Table 15. Index 1 in $z_{D,1}$ and $\theta_{D,1}$ refers to Setup 1, while index 2 in $z_{D,2}$ and $\theta_{D,2}$ refers to Setup 2. A negative sign in the heave motion indicates downward movement of the ship, while a negative sign in the pitch motion indicates trim by the stern.

Table 13 Results of Lucy Ashton case (full-scale – λ=1, Setup 1)

Fr [-]	$C_{T,\mathrm{EFD}}\cdot 10^3$ [-]	$C_{T,\mathrm{CFD}}\cdot 10^3$ [-]	E %D
0.130	2.278	2.287	−0.4
0.173	2.259	2.214	2.0
0.219	2.566	2.570	−0.2
0.260	3.024	3.101	−2.6
0.304	4.165	4.336	−4.1

Table 14 Results of Lucy Ashton case (full-scale – λ=1, Setup 2)

Fr [-]	$C_{T,\mathrm{EFD}}\cdot 10^3$ [-]	$C_{T,\mathrm{CFD}}\cdot 10^3$ [-]	E %D
0.130	2.278	2.302	−1.0
0.173	2.259	2.287	−1.2
0.219	2.566	2.556	0.4
0.260	3.024	3.177	−5.1
0.304	4.165	4.402	−5.7

Table 15 Dynamic motions and relative comparison of them between Setup 1 and Setup 2

Fr [-]	$z_{D,1}$ [m]	$\theta_{D,1}$ [deg]	$z_{D,2}$ [m]	$\theta_{D,2}$ [deg]	δz_D [%]	$\delta\theta_D$ [%]
0.130	−0.014	−0.011	−0.014	−0.005	0.0	54.5
0.173	−0.027	−0.019	−0.026	−0.012	3.7	36.8
0.219	−0.048	−0.038	−0.047	−0.031	2.1	18.4
0.260	−0.074	−0.084	−0.072	−0.082	2.7	2.4
0.304	−0.111	−0.206	−0.109	−0.194	1.8	5.8

The grid uncertainty analysis was performed for Setup 1 and the maximum considered speed (Fr=0.304), using three different cell sizes to generate the coarse, medium and fine meshes. The resulting total resistance coefficients obtained from these three mesh densities, along with the corresponding number of cells in the computational domain covering the half-hull, are presented in Table 16.

Table 16 Grid uncertainty analysis (λ=1, Fr=0.304)

	Coarse (S_3)	Medium (S_2)	Fine (S_1)
$C_{T,\mathrm{CFD}}$ x 10^3 [-]	4.336	4.207	4.128
No. of cells x 10^6	0.846	1.633	3.481

Grid uncertainty in this case is 5.3% and since it is bigger than comparison error (4.1%), the validation is achieved.

4. Discussion

All EFD and CFD results listed in Tables 6–11 and Tables 13–14 are presented graphically in Fig. 2 as functions of the Reynolds number, plotted on a logarithmic scale. The solid lines represent the CFD-predicted total resistance coefficients obtained with Setup 1, the dashed lines correspond to the experimental data, and the dotted line denotes the full-scale CFD results obtained with Setup 2. The long dash dotted line represents ITTC 1957 friction line. This graphical comparison provides a clear assessment of the consistency between CFD and EFD results across all geometric scales, particularly at higher speeds.

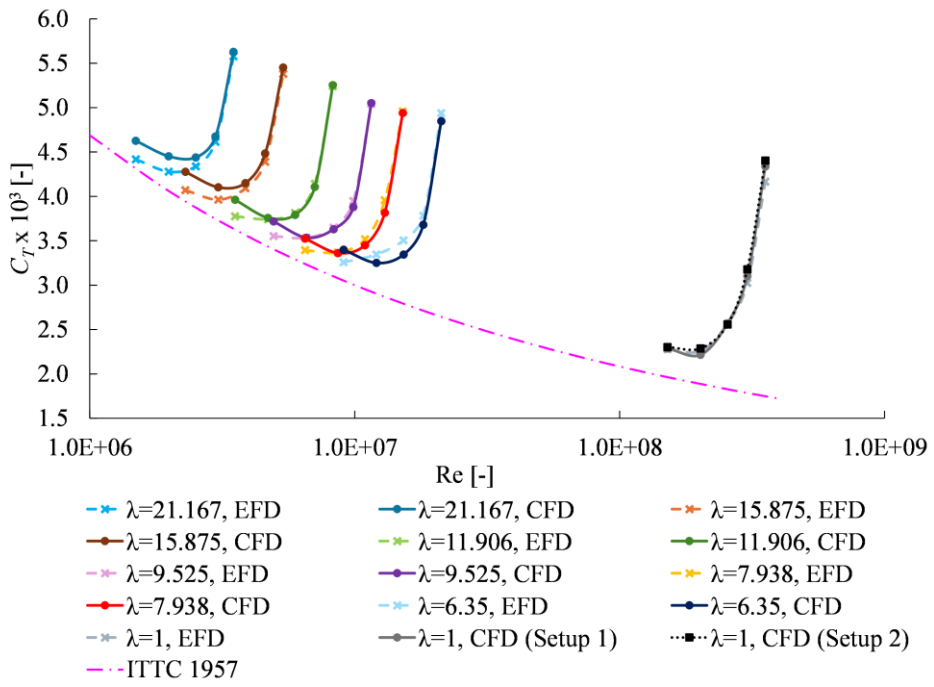

Fig. 2 Total resistance coefficients for all geometric scales

The largest discrepancies between CFD predictions and experiments occur at the lowest speed (*Fr*=0.130) for all model scales. This systematic behaviour suggests that the turbulence-modelling strategy may require adjustment for low-speed conditions. It should be noted that the same simulation configuration, Setup 1, was used for all scales and all Froude numbers.

The main distinction between Setup 1 and Setup 2 is the inclusion of the surge degree of freedom in Setup 2. Instead of prescribing a uniform inflow velocity, a reference point was attached to the hull and allowed to move relative to the vessel while being subjected to a thrust force. This formulation was used to emulate the effect of the jet engines installed on the deck during the full-scale tests.

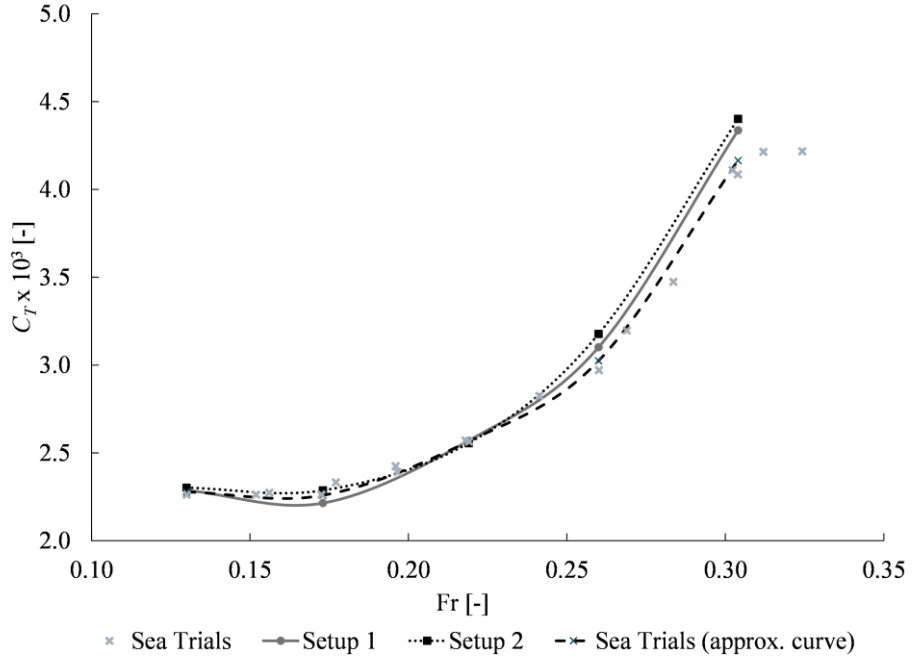

Fig. 3 Total resistance coefficients for full-scale. Sea Trials (EFD) data and CFD data based on Setup 1 and Setup 2 approaches

Fig. 3 presents the full-scale total resistance coefficients only as a function of *Fr*: the experimental measurements (tabulated values, marked with ‘x’), the fitted polynomial (dashed line), and the CFD results

obtained using Setup 1 (solid line) and Setup 2 (dotted line). A closer agreement between CFD and EFD results is observed at lower speeds, while the differences increase at higher speeds. Despite employing two fundamentally different modelling approaches, both setups produce comparable predictions of the total resistance.

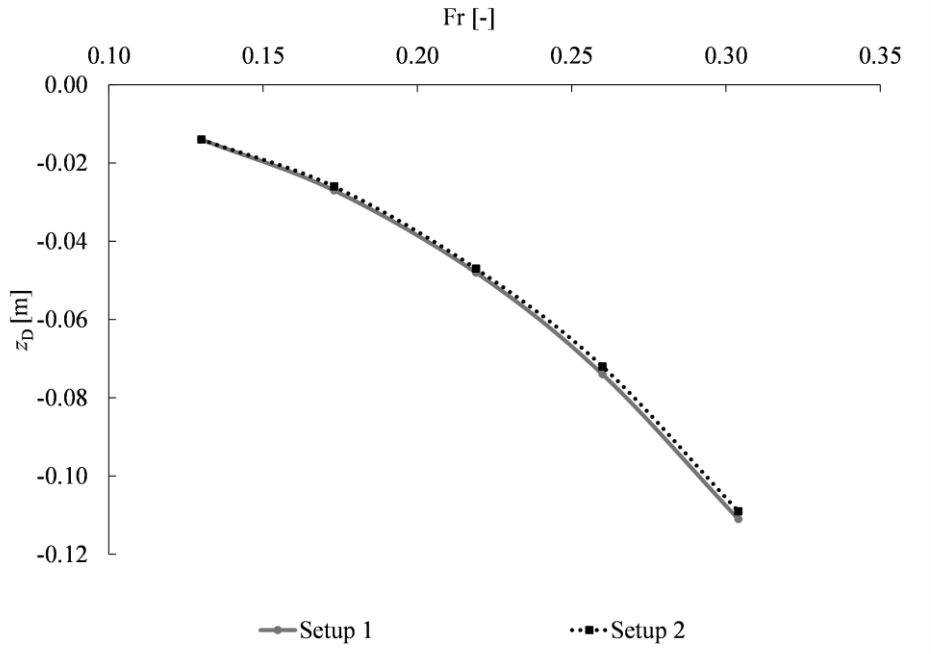

Fig. 4 Dynamic heave. Comparison between Setup 1 and Setup 2

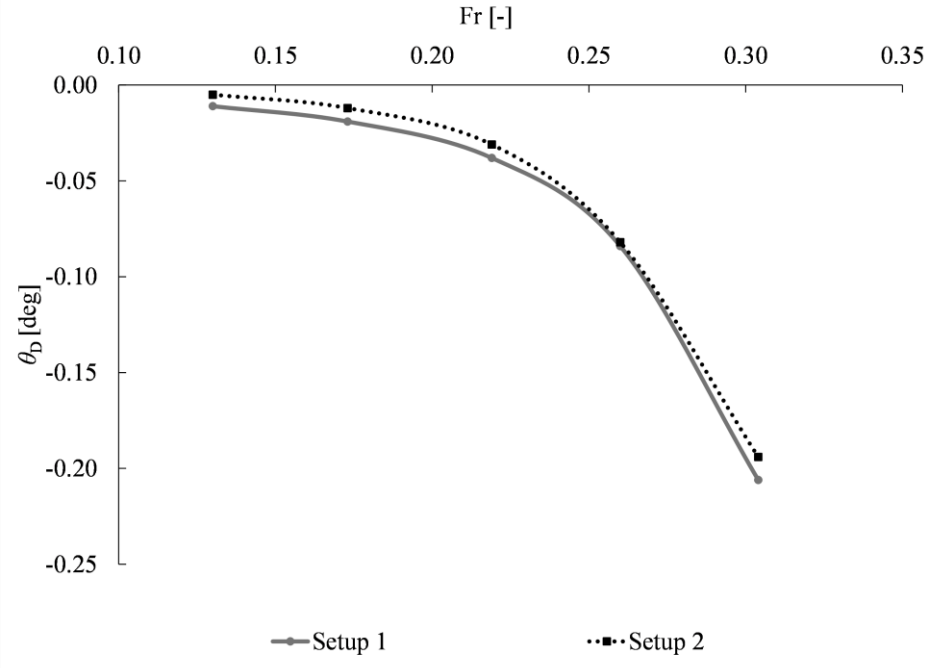

Fig. 5. Dynamic pitch. Comparison between Setup 1 and Setup 2

Because Lucy Ashton was originally propelled by large paddle wheels mounted on the sides, it is reasonable to examine whether the shift in the location and type of thrust affects the dynamic motions (heave and pitch). Mechanically, the moment generated by the deck-mounted jet thrust differs from that produced by the paddle-wheel blades, which could influence the vessel's response. However, the CFD results show that both modelling approaches (Setup 1 and Setup 2) produce similar trends in heave and pitch, as shown in Fig. 4 and Fig. 5. Moreover, the configuration with deck-mounted jets results in slightly smaller dynamic motions.

The magnitude of these differences is negligible in practice. Although the relative difference in heave reaches up to 4%, the physical displacement is only about 2 mm. For pitch, the relative deviation at the lowest speed is around 55%, yet the absolute value remains extremely small, on the order of 10^{-3} degrees, indicating that the effect is practically insignificant for resistance evaluation.

Both setups show a standard deviation of approximately 2% when compared with the experimental data. Considering that the standard deviation introduced by recalculating the full-scale resistance into the non-dimensional total resistance coefficient at a given Froude number is 3.1%, the results strongly suggest that both CFD approaches are robust. The difference in how thrust is applied (paddle-wheel mechanism versus jet-thrust representation) does not meaningfully affect the predicted total resistance, and both setups can be considered reliable for assessing full-scale hydrodynamic performance.

5. Conclusion

This study aimed to evaluate total resistance coefficient estimation for unique ship hull using CFD simulations. The research encompassed Lucy Ashton, for which the resistance measurements in six different model scales and in full scale are available. A focus on investigating is how scaling, *Fr* number and *Re* number affect total resistance predictions.

The resistance coefficient validation demonstrated that CFD simulations yielded results with an error margin within about 5% when compared to experimental data. The total resistance coefficient deviations fall within accepted industry tolerances for CFD validation (typically ±5%).

The comparison of two simulation strategies for the full scale (Setup 1 and Setup 2) showed that the difference in thrust modeling, uniform inflow versus thrust-driven surge, does not significantly influence the predicted total resistance. Although noticeable relative deviations appear in small dynamic motions such as heave and pitch, their absolute magnitudes remain extremely small (on the order of millimeters or 10^{-3} degrees). Both setups achieve a standard deviation of approximately 2% when compared with the fitted experimental values, confirming the robustness of the CFD methodology.

Despite the encouraging results, several limitations should be acknowledged. The standard deviation of the fitted polynomial is approximately 3%, which is more than twice the 1.3% deviation observed between the two estimation methods. This indicates that the methods are mutually consistent with relatively small and stable differences, whereas the larger scatter relative to the polynomial suggests that the approximation model is not optimal or that the data exhibit nonlinear behavior that the chosen polynomial cannot adequately capture. The largest discrepancies occur at the lowest speeds (Fr = 0.130), suggesting that the turbulence model or near-wall treatment may require refinement for these flow regimes for each scale. There is also concern about possible turbulence triggering in the model scale experiments at lower speeds, since this aspect is not described in the reports and CFD well predict total resistance in a full-scale condition at lower speeds. Only one CFD code (STAR-CCM+) and one general meshing approach were used; cross-validation using alternative solvers or mesh-generation technologies was not performed.

Future work should focus on improving turbulence-modeling strategies for low-speed regimes. Extending the grid-convergence analysis to a broader range of *Fr* numbers would further strengthen the numerical validation. Finally, incorporating scale effects through advanced wall-modeling or hybrid RANS–LES approaches could provide additional view into the sources of discrepancy between model- and full-scale predictions.

Overall, the results confirm that both CFD approaches used in this study are reliable for estimating the total resistance of the Lucy Ashton hull across all scales, supporting the broader applicability of CFD as a predictive tool in ship hydrodynamics, especially in full-scale.

NOMENCLATURE

∇	m^3	Displacement volume
B	m	Breadth
C	-	Additive constant
C_b	-	Block coefficient
C_m	-	Midship coefficient
C_p	-	Prismatic coefficient
C_T	-	Total resistance coefficient
$C_{T,\mathrm{CFD}}$	-	Total resistance coefficient based on CFD analysis
$C_{T,\mathrm{EFD}}$	-	Total resistance coefficient based on EFD analysis
D	-	EFD data
E	-	Comparison error
Fr	-	Froude number
FS	-	Factor of safety
H	m	Depth
K	-	Von Karman constant
k_s	m	Surface roughness
L_{pp}	m	Length between perpendiculars
L_{wl}	m	Waterline length
P	-	Distance metric to the asymptotic range
p_{RE}	-	Order of accuracy
p_{th}	-	theoretical order of accuracy
R	-	Convergence ratio
Re	-	Reynolds number
S	-	CFD solution
T	m	Draft
U_D	-	Data uncertainty
U_G	-	Grid uncertainty
U_{SN}	-	Numerical uncertainty
U_V	-	Validation uncertainty
WDL	m	Wave damping length
WS	m^2	Wetted surface without rudder
WS_{total}	m^2	Wetted surface with rudder
z_{D}	m	Dynamic heave
$\Delta_{(\mathrm{sw})}$	t	Displacement in sea water
ΔC_F	-	Roughness allowance
δ_{RE}	-	Error estimate
δz_{D}	%	Relative change in dynamic heave
$\delta\theta_{\mathrm{D}}$	%	Relative change in dynamic pitch
ε_{21}	-	Difference between solutions obtained using medium and fine mesh
ε_{32}		Difference between solutions obtained suing coarse and medium mesh
η_a	kg/ms	Dynamic viscosity of air
η_w	kg/ms	Dynamic viscosity of water

θ_D	deg	Dynamic pitch
λ	-	Scale
π	-	Pie
ρ_a	kg/m^3	Air density
ρ_w	kg/m^3	Water density
υ	m^2/s	Kinematic viscosity of water

ABBREVIATIONS

AI	Artificial Intelligence
ANN	Artificical Neural Network
CFD	Computational Fluid Dynamics
EEXI	Energy Efficiency for Existing Ship Index
EFD	Experimental Fluid Dynamics
GCI	Grid Convergence Index
GHG	Greenhouse Gas
HRIC	High-Resolution Interface Capturing
IMO	International Maritime Organization
ITTC	International Towing Tank Conference
KCS	KRISO Container Ship
KVLCC2	KRISO Very Large Crude Carrier 2
RKE	Realizable k-ε (turbulence model variant)
RSM	Reynolds Stress Model
SST	Shear Stress Transport (turbulence model)
SSTKO	Shear Stress Transport (variant of SST model)
VOF	Volume of Fluid

ACKNOWLEDGMENTS

The research is supported by Ministry of Science, Technology Development and Innovation of Republic of Serbia, Contract No. 451-03-137/2025-03/200105. Authors would like to acknowledge Ocean Pro Marine Engineers LTD for its help in guidance and support for CFD assessment.

REFERENCES

[1] IMO, 2018. Resolution MEPC.304(72). Initial IMO Strategy on Reduction of GHG Emissions from Ships. IMO, London, England. URL https://docs.imo.org/. (accessed 5th March 2025)

[2] IMO, 2023. Resolution MEPC.377(80). 2023 IMO Strategy on Reduction of GHG Emissions from Ships. IMO, London, England. Available online. https://docs.imo.org/. (Accessed 5th March 2025)

[3] IMO, 2014. Third IMO Greenhouse Gas Study 2014. https://www.imo.org/. (accessed 5th March 2025)

[4] IMO, 2021. Fourth IMO Greenhouse Gas Study 2020. https://www.imo.org/. (accessed 5th March 2025)

[5] Statista, 2025. https://www.statista.com/statistics/1185535/transport-carbon-dioxide-emissions-breakdown/, (accessed 5th March 2025)

[6] Zhi-Rong, Z., Hui, L., Song-Ping, Z., Feng, Z., 2006. Application of CFD in ship engineering design practice and ship hydrodynamics. *Journal of Hydrodynamics*, 18(3), 315-322. https://doi.org/10.1016/S1001-6058(06)60072-3

[7] Tang, H., Zhu, R., Wan, Q., Ren, D., 2025. Short-term prediction of trimaran load based on data driven technology. *Brodogradnja*, 76 (1), 76101. https://doi.org/10.21278/brod76101

[8] Meng, L., Gan, H., Liu, H., Lu, D., 2025. Deep learning-based research on fault warning for marine dual fuel engines. *Brodogradnja*, 76 (3), 76303. https://doi.org/10.21278/brod76303

[9] Xiao, G., Yang, D., Xu, L., Li, J., Jiang, Z., 2024. The Application of Artificial Intelligence Technology in Shipping: A Bibliometric Review. *Journal of Marine Science and Engineering*, 12, 624. https://doi.org/10.3390/jmse12040624

[10] Guo, S., Zhang, B., Tian, Z., Liu, J., Tang, H., 2024. Automatic Optimal Design Method for Minimum Total Resistance Hull Based on Enhanced FFD Method. *Brodogradnja*, 74 (4), 75407. https://doi.org/10.21278/brod75407

[11] ITTC, 2021. 7.5-02-03-01.4. 1978 ITTC Performance Prediction Method, ITTC Quality System Manual, Recommended Procedures and Guidelines; International Towing Tank Conference, *Propulsion Committee of the 29th ITTC*. https://www.ittc.info/media/8017/75-02-03-014.pdf (accessed 6th March 2025)

[12] IMO, 2022. Resolution MEPC.350(78). 2022 Guidelines on the Method of Calculation of the Attained Energy Efficiency Existing Ship Index (EEXI). IMO, London, England. https://docs.imo.org/ (accessed 6th March 2025)

[13] IMO, 2022. Resolution MEPC.351(78). 2022 Guidelines on Survey and Certification of the Attained Energy Efficiency Existing Ship Index (EEXI). IMO, London, England. https://docs.imo.org/ (accessed 6th March 2025)

[14] IACS, 2024. EEXI Implementation Guidelines, Recommendation No. 172. London, England. https://iacs.org.uk (6th March 2025)

[15] ITTC, 2024. 7.5-03-02-02. Benchmark Database for CFD Validation for Resistance and Propulsion, ITTC Quality System Manual, Recommended Procedures and Guidelines; International Towing Tank Conference, *Specialist Committee on Combined CFD-EFD Methods of 30th ITTC.* https://www.ittc.info/media/11956/75-03-02-02.pdf (accessed 6th March 2025)

[16] Ponkratov, D., 2016. The workshop in ship scale computer simulations, Proceedings, Lloyd's Register, Southampton, UK

[17] Ponkratov, D., Zegos C., 2014. Ship Scale CFD SelfPropulsion Simulation and Its Direct Comparison with Sea Trials Results, *International Conference on Computational and Experimental Marine Hydrodynamics MARHY'14*, Chennai, India

[18] Ponkratov, D., Zegos, C., 2015. Validation of ship scale CFD self-propulsion simulation by the direct comparison with sea trials results. *Proceedings of the Fourth International Symposium on Marine Propulsors*. SMP'15, Austin, Texas, USA, June 2015

[19] Huang, L., Pena, B., Thomas, G., 2023. Towards a full-scale CFD guideline for simulating a ship advancing in open water. *Ship Technology Research*, 70(3), 222–238. https://doi.org/10.1080/09377255.2023.2167537

[20] ITTC, 2024. 7.5-03-01-01. Uncertainty Analysis in CFD Verification and Validation, Methodology and Procedures, ITTC Quality System Manual, Recommended Procedures and Guidelines; International Towing Tank Conference, *Specialist Committee on Combined CFD-EFD Methods of 30th ITTC*. https://www.ittc.info/media/11950/75-03-01-01.pdf (accessed on 06.03.25.)

[21] Jasak, H., Vukčević, V., Gatin, I., Lalović, I, 2019. CFD validation and grid sensitivity studies of full scale ship self-propulsion, *International Journal of Naval Architecture and Ocean Engineering*, 11(1), 33-43. https://doi.org/10.1016/j.ijnaoe.2017.12.004

[22] Pena, B., Muk-Pavic, E., Fitzsimons, P., 2020. Detailed analysis of the flow within the boundary layer and wake of a full-scale ship, *Ocean Engineering*, 218, 108022. https://doi.org/10.1016/j.oceaneng.2020.108022

[23] Luo, W., Yang, B., Sun, Y., 2021. Hydrodynamic analysis of KVLCC2 ship sailing near inclined banks. *Mathematical Problems in Engineering*, 2021, 655971. https://doi.org/10.1155/2021/6655971

[24] Mikulec, M., Piehl, H., 2023. Verification and validation of CFD simulations with full-scale ship speed/power trial data. *Brodogradnja*, 74(1), 41-62. https://doi.org/10.21278/brod74103

[25] Saydam, A. Z., Küçüksu, G. N., İnsel, M., Gökçay, S., 2022. Uncertainty quantification of self-propulsion analyses with rans-cfd and comparison with full-scale ship trials. *Brodogradnja*, 73(4), 107-129. https://doi.org/10.21278/brod73406

[26] Farkas, A., Degiuli, N., Martić, I., 2018. Assessment of hydrodynamic characteristics of a full-scale ship at different draughts. *Ocean Engineering*, 156, 135–152. https://doi.org/10.1016/j.oceaneng.2018.03.002

[27] Orych, M., Werner, S., Larsson, L., 2021, Validation of full-scale delivered power CFD simulations, *Ocean Engineering*, 238, 109654. https://doi.org/10.1016/j.oceaneng.2021.109654

[28] Castro A. M., Carrica P., M., Stern F., 2011. Full scale self-propulsion computations using discretized propeller for the KRISO container ship KCS, *Computers & Fluids*, 51(1), 35-47. https://doi.org/10.1016/j.compfluid.2011.07.005

[29] Farkas, A., Degiuli, N., Martić, I., Dejhalla, R., 2019. Numerical and experimental assessment of nominal wake for a bulk carrier. *Journal of Marine Science and Technology*, 24, 1092–1104. https://doi.org/10.1007/s00773-018-0609-4

[30] Denny, M. E., 1951. B.S.R.A. Resistance Experiments on the Lucy Ashton, Part I – Full Scale Measurements, *International Conference of Naval Architects and Marine Engineers 1951*, Unwin Brothers, 40-57

[31] Schuster, S., 1969. Schiffstechnische Meßfahrten mit dem Forschungsschiff "Meteor" 1967. Meteor Forschungsergebnisse: Reihe A, Allgemeines, *Physik und Chemie des Meeres*, 5, 72-84

[32] Conn, J. F. C., Lackenby, H., Walker, W. P., 1953. B.S.R.A. Resistance Experiments on the Lucy Ashton, Part II – The Ship-Model Correlation for the Naked Hull Conditions, *Spring Meeting of the Institution of Naval Architects*, March 25, 1953, 350-436

[33] Lackenby, H., 1955. Resistance Experiments on the Lucy Ashton, Part III – The Ship-Model Correlation for the Shaft-Appendage Conditions, *Quartetly Transactions of the Institution of Naval Architects*, 97(2), 109-166

[34] Smith, L., 1955. Resistance Experiments on the Lucy Ashton, Part IV – Miscellaneous Investigations and General Appraisal, *Quartetly Transactions of the Institution of Naval Architects*, 97(4), 525-561

[35] Lopes, R., Eslamdoost, A., Johansson, R., RoyChoudhury, S., Bensow, R. E., Hogstrom, P., Ponkratov, D., 2025. Resistance prediction using CFD at model- and full-scale and comparison with measurements, *Ocean Engineering*, 321, 120367. https://doi.org/10.1016/j.oceaneng.2025.120367

[36] Lopes, R., Eslamdoost, A., Bensow, R. E., Ponkratov, D., Kompe, A., Geremia, P., Pekküçük, Ç. B., et al. 2026. A summary of the Lucy Ashton resistance prediction workshop, *Ocean Engineering*, 343, 122951. https://doi.org/10.1016/j.oceaneng.2025.122951

[37] Hirt, C.W., Nichols, B.D., 1981. Volume of Fluid (VOF) Method for the Dynamics of Free Boundaries. *Journal of Computational Physics*, 39, 201-225. https://doi.org/10.1016/0021-9991(81)90145-5

[38] Menter, F. R., 1994. Two-equation eddy-viscosity turbulence models for engineering applications, *AIAA journal*, 32(8), 1598-1605. https://doi.org/10.2514/3.12149

[39] Roache, P. J., 1998, Verification and Validation in Computational Science and Engineering, *Hermosa publishers*, Albuqurque, New Mexico

[40] Xing, T., Stern, F., 2010, Factors of Safety for Richardson Extrapolation, *Journal of Fluids Engineering*, 132(6), 061403. https://doi.org/10.1115/1.4001771

[41] ITTC, 2024. 7.5-03-02-04, Practical Guidelines for Ship Resistance CFD, ITTC Quality System Manual, Recommended Procedures and Guidelines; International Towing Tank Conference, *Specialist Committee on Combined CFD-EFD Methods of 30th ITTC*. https://www.ittc.info/media/11960/75-03-02-04.pdf (accessed 11th March 2025)

[42] ITTC, 2024. 7.5-03-03-01, Practical Guidelines for Ship Self-Propulsion CFD, ITTC Quality System Manual, Recommended Procedures and Guidelines; International Towing Tank Conference, *Specialist Committee on Combined CFD-EFD Methods of 30th ITTC*. https://www.ittc.info/media/11964/75-03-03-01.pdf (accessed 11th March 2025)